Postprint. Jing Deng, et al., Chemistry of Materials, 2020, 32, 10, 4174-4184.
https://doi.org/10.1021/acs.chemmater.0c00020

# Morphologically tunable MOF nanosheets in mixed matrix membranes for $CO_2$ separation

Jing Deng[†1], Zhongde Dai[†1], Jingwei Hou[2] and Liyuan Deng[*1]

AUTHOR ADDRESS

[1] Department of Chemical Engineering, Norwegian University of Science and Technology Trondheim, 7491, Norway.

Email: deng@nt.ntnu.no

[2] School of Chemical Engineering, Faculty of Engineering, Architecture and Information Technology, the University of Queensland, Brisbane, Queensland, Australia

† These authors contributed equally

**ABSTRACT:** This study first develops a facile method to synthesize zeolitic imidazolate framework cuboid (ZIF-C) nanosheets with tunable thickness from 70 nm to 170 nm from an aqueous polymer solution. The obtained ZIF-C nanosheets were characterized by various techniques, including X-Ray Diffractometer (XRD), Scanning Electron Microscope (SEM), Atomic Force Microscopy (AFM), Fourier-Transform Infrared Spectroscopy (FTIR), X-ray Photoelectron Spectroscopy (XPS), $N_2$ adsorption and Thermogravimetric analysis (TGA), to understand their compositional and structural properties. The synthesized ZIF-Cs nanosheets with different thicknesses were further applied as nanofillers to prepare Pebax-based mixed matrix membranes (MMMs) to study the effect of the morphology on membrane properties and $CO_2/N_2$ separation performances under different relative humidity conditions. Results reveal that the incorporation of these ZIF-Cs simultaneously enhances $CO_2$ permeability and $CO_2/N_2$ selectivity in the mixed matrix membranes. In addition, MMMs with the thickest ZIF-C nanosheet presents better performance. A $CO_2$ permeability of 387.2 Barrer accompanied with a $CO_2/N_2$ selectivity of 47.1 has been documented, nearly doubled in $CO_2$ permeability with slightly increased selectivity compared with membranes containing thinner nanosheets.

## INTRODUCTION

Owing to the intrinsic porous structures, metal–organic frameworks (MOFs), a class of crystalline materials constituted of metal ions/clusters linked by organic ligands, have drawn extensive attentions in diverse fields during the past decades, such as energy storage, catalysis and separation/storage.[1-4] The nanoscale caves with tunable sizes (from angstrom to nanometre range), high surface area and adjustable surface make them promising as molecular sieving materials to overcome the trade-off relationship[5] between permeability and selectivity of traditional polymeric membranes, which also known as the Robeson upper bound.[3, 6-8] Therefore, enormous effort has been devoted to developing new MOFs and MOF-based membranes aiming for enhanced separation performances.[9-13]

Incorporating MOFs into polymeric membranes to fabricate mixed matrix membranes (MMMs) is one of the most studied approaches considering the combination of the processability of polymeric substrates and the molecular sieving capability of MOFs, the advantages from both sides.[2, 14, 15] For instance, Bae *et al.* reported that the addition of sub-micrometer zeolitic imidazolate framework (ZIF) -90 into 6FDA-DAM realized around 85% and 61% increment in $CO_2$ permeability (from 390 to 720 Barrer) and $CO_2/CH_4$ selectivity (from 24 to 37), respectively.[16] In another work reported by Hwang et al., the $CO_2$ permeability benefits an 8.9-fold enhancement (70 to 623 Barrer), with a slight loss in selectivity.[17] This significant gain in $CO_2$ permeation is contributed by the increased $CO_2$ diffusivity from the hollow structure of fillers, the pore inside ZIF-C crystals, and the enhanced solubility from the imidazole organic linkers.

Despite these great improvements, the performances of the majority of the MMMs are still far below the theoretically predicted values.[1, 3, 8, 18-21] Among various reasons, the filler geometry is a crucial factor affecting the interfacial morphology between fillers and the polymer matrix.[22] Sphere [23, 24] is the most common shape of the fillers used in MMMs. Researchers have found that the size of fillers has a significant influence on the final performance of MMMs. As a rule of thumb, MOFs with smaller sizes have higher external surface areas, and thus, larger interfacial areas between polymer and nanoparticles can be anticipated. However, the fabrication of highly crystalline MOF nanoparticles is thermal-dynamically unfavourable and technically challenging. On the other hand, the tendency of agglomeration for small particles is more significant than their larger analogies, leading to poor filler dispersion.[25-27] Therefore, the optimization of nanoparticle size should be taken into consideration. Zheng

*et al.* prepared a series of MMMs containing Pebax and ZIF-8 nanoparticles with different sizes (40 – 110 nm) and found out that the larger nanoparticles are preferable for both $CO_2$ permeability and $CO_2/N_2$ selectivity, with the studied ZIF-8 loadings.[27] It is believed that the presence of larger ZIF-8s in MMMs leads to a higher free volume and thus higher permeability, and the higher specific surface area of ZIF-8 nanoparticles benefits the selectivity. Similar results have been reported in several research works,[25, 26] but further increases in particle size may not bring positive results; the visible sedimentation of particles inside membranes and the voids between fillers and polymer matrix were observed in MMMs containing 10 wt.% MIL-53(Al) particles with a size of 3.2 µm. [28]

Very recently, MOFs with a higher aspect ratio, such as sheet-, flake-, or platelet-like MOFs, have been considered as potentially more promising fillers due to the increased permeation resistance for rejected gas (and hence the enhanced separation factor) as well as the shortcut path for desired molecules (and therefore the elevated flux).[21, 23, 29-31] However, only limited literature can be found applying MOF nanosheets in MMMs for gas separation applications.[18, 19, 32-34] Gascon and co-workers[18] synthesized 2D copper 1,4-benzenedicarboxylate (CuBDC) nanosheets with the thicknesses of 5 – 25 nm and added them into Matrimid membranes. The resultant MMMs display an improved $CO_2/CH_4$ selectivity (30 – 80%) compared to the neat polymer. Moreover, the presence of the nanosheets counteracts the plasticization due mainly to the superior separation performance of the 2D structure. It is worth mentioning that the MMMs containing bulk or nanocrystal CuBDC do not display this enhanced performance. Under the same conceptual framework, Zhao *et al.* also found similar results in membranes comprising of PBI and $[Cu_2(ndc)_2(dabco)]$ nanosheets for $H_2/CO_2$ separation.[20] Wang and co-workers employed two-dimensional ZIF-L into polyimides; the incorporation of ZIF-L into the membrane greatly improved both the $H_2$ permeability and $H_2/CO_2$ selectivity.[31]

The above studies have revealed the great potential of MMMs with lamellar MOFs as nanofillers. Up to now, most of the MOF nanosheets were prepared via a top-down or bottom-up approach.[29] The top-down method normally refers to exfoliating lamellar MOF sheets from bulky MOFs by mechanical forces (e.g., ultrasonication), while the bottom-up approach means a direct synthesis of lamellar MOFs by precisely controlling the reaction conditions (e.g., adjusting solvents or employing surfactants). Despite the diversity of synthesis methods developed for lamellar MOFs, a facile and economical way of synthesis lamellar MOFs with controllable thickness and morphology is still highly desirable.

Hence, in this work, a simple fabrication method for ZIF cuboids (ZIF-Cs) nano-sheets was developed for the first time. The reaction was conducted in an aqueous solution at room temperature with the presence of poly(vinyl alcohol) (PVA) in addition to the ZIF precursors (zinc ions and imidazolate ligands). The material properties of the as-synthesized ZIF-Cs were analyzed by various characterization approaches: Scanning Electron Microscope (SEM), Atomic Force Microscopy (AFM), Fourier-Transform Infrared Spectroscopy (FTIR), X-ray Photoelectron Spectroscopy (XPS), $N_2$ adsorption and X-Ray Diffractometer (XRD). Later, these ZIF-Cs were incorporated into Pebax 1657 to study their influences on morphology, chemistry nature and crystallinity of MMMs. Mixed gas permeation tests were conducted to reveal the impact of nanocuboids thicknesses on the $CO_2$ separation performance of resultant MMMs.

## EXPERIMENTAL

## MATERIALS

$Zn(NO_3)_2{\cdot}6H_2O$ and 2-methylimidazole (Hmim) were purchased from Sigma, Norway. Poly(vinyl alcohol) (PVA, Mn= 30000 – 70000, 72000, and 85000 – 124000 g/mol) were ordered from Sigma, Germany. Pebax 1657 pellets were ordered from Arkema, France. Ethanol (96%) was purchased from VWR, Norway. All the chemicals were used without further treatment.

## ZIF-C SYNTHESIS

In brief, PVA was dissolved in DI water at 80 °C with reflux to prepare 1 wt.% PVA solution. After the solution cooled down to room temperature, 0.59 g $Zn(NO_3)_2{\cdot}6H_2O$ and 1.32 g of Hmim were added into 40 ml PVA solution, respectively. After the $Zn(NO_3)_2{\cdot}6H_2O$ and Hmim had been fully dissolved, the two solutions were mixed, and the reaction was carried out at room temperature for 3 hours. Afterwards, the ZIF-C was separated using a centrifuge with 10000 rpm for 10 mins. Obtained ZIF-C particles were re-dispersed in DI water and centrifuged two times more to remove the residual PVA. Finally, the ZIF-C particles were dispersed in DI water to prevent possible aggregation. The ZIF-C content in the dispersion was calculated by drying 0.5g of the dispersion at 40 °C in a vacuum oven for 1 night. Three PVAs with different molecular weights have been used; hence the ZIF-Cs prepared from PVA with a molecular weight of XX are defined as "ZIF-C XX".

## MEMBRANE PREPARATION

MMMs were prepared through a knife-casting method similar to those in the literature.[35] Typically, Pebax 1657 was dissolved in $EtOH/H_2O$ mixture (70/30 vol%) with reflux at 80 °C for ~ 3 hours with a concentration of 8 wt.%. Pebax solution was mixed with the desired amount of ZIF-C aqueous dispersion under stirring for at least 6 hours. The mixture was then cast on a glass plate using a casting knife (PA-4302, BYK-CHEMIE GMBH, Germany) with a wet gap of ~ 600 µm. The cast membrane was then placed in a ventilated oven at 40 °C for at least 6 hours. After the membrane was removed from the glass plates, it was dried in a vacuum oven at 60 °C for another 6 hours before further characterization.

## CHARACTERIZATION

The topography of ZIF-C nanosheets was characterized by an AFM (Dimension Icon, Bruker) using the ScanAsyst mode. The as-prepared nanosheets were dispersed in ethanol and dried on microscope cover glasses for AFM analysis. An SEM (TM3030 tabletop microscope, Hitachi) was also employed for the morphology study of these ZIF-C nanosheets and the resultant MMMs. For MMMs, cross-section specimens were obtained by breaking the samples in liquid $N_2$. A sputter coating with gold (2 mins) was conducted for all samples before SEM characterization.

The thermal stability tests for the ZIF-C nanosheets and the MMMs were performed by employing a TGA (TG 209F1 Libra, Netzsch). Samples with a weight of 10 – 20 mg were used. All samples

were heated from room temperature to 800 °C with a heating rate of 10 °C / min. $N_2$ was used as both protective and sweep gas.

A Tristar II 3020 (Micromeritics Instruments, USA) was used for $N_2$ sorption isotherms. Before the measurements, ZIF-C samples were degassed at room temperature overnight with vacuum.

The crystallinity of the prepared nanosheets and MMMs was analyzed by a Bruker D8 A25 DaVinci X-ray Diffractometer (Bruker) with characteristic wavelength λ=1.54 Å (Cu Kα radiation). The scans were taken in the 2θ range from 5° to 75°.

FTIR spectroscopy was performed employing a Thermo Nicolet Nexus spectrometer. The obtained spectra were an average of 16 scans with wavenumber from 550 $cm^{-1}$ to 4000 $cm^{-1}$.

X-ray photoelectron spectroscopy (XPS) was performed on a PHI-560 ESCA (Perkin Elmer) using a nonmonochromatic Mg Kα excitation source at 15 kV. The C 1s peak position was set to 284.6 eV as an internal standard.

Gas permeation performance of MMMs was conducted using a mixed-gas permeation setup reported in our previous work.[35, 36] Feed gas was the $CO_2/N_2$ (10/90 vol%) gas mixture, whereas pure $CH_4$ was used as the sweep gas. The water vapor was introduced by humidified feed and sweep gas, and the humid gases were mixed with dry gases with accurate flow ratio to achieve the desired humidity. All gas permeation tests were carried out at room temperature with a feed pressure and sweep pressure of 2.0 and 1.05 bar, respectively. The compositions of permeate and retentate streams were analyzed by a calibrated gas chromatograph (490 Micro GC, Agilent) throughout the tests.

The permeability coefficient (*Pi*) of the *i*th penetrant species can be calculated from equation (1):

$$P_i = \frac{N_{perm}\left(1 - y_{H_2O}\right)y_i}{A\left(p_{i,feed} - p_{i,perm}\right)} \quad (1)$$

where $N_{perm}$ is the total permeate flow measured by a bubble flow meter (ml/min), $y_{H_2O}$ refers to the molar fraction of the water in the permeate flow (calculated according to the relative humidity value and the vapor pressure at the tested temperature), $y_i$ is the molar fraction of the gas i in the permeate flow (%), and $p_{i,feed}$ and $p_{i,perm}$ stand out the partial pressures of the gas *i* in feed and permeate streams, respectively. In the present work, the gas permeability is expressed in the unit of Barrer (1 Barrer = $10^{-10}$ $cm^3(STP)\cdot cm\cdot cm^{-2}\cdot s^{-1}\cdot cmHg^{-1}$). The separation factor was determined from equation (2):

$$\alpha_{AB} = \frac{y_A/y_B}{x_A/x_B} \quad (2)$$

where $y_A$ and $y_B$ are the mole ratio of gas A and B in the permeate stream, while $x_A$ and $x_B$ are the mole ratio of gas A and B in the feed side.

## RESULTS AND DISCUSSION

### ZIF-C SYNTHESIS AND CHARACTERIZATION

It is well-known that additives, such as small molecules,[37] surfactants,[38-41] or polymers, [42-44] play a very important role on nanoparticle morphology because of the competition of the reactants between other reactants and the additives, the adjusted pH, and the restricted regions for crystal growth or selective absorption.[45] To investigate the effect of PVA addition on the formation of ZIF-Cs, the morphologies and material properties of the as-prepared ZIF-Cs were characterized via various technics, and the results are shown in **Figure 1, Figure S1-S2** and **Table S1-S2**. The XRD curves of these ZIF-C generated in PVA solution have almost identical patterns with the one from $H_2O$ [46], as shown in **Figure 1 (F)**, suggesting that the obtained product has the same crystal structure with the ZIF-L, and the presence of PVA does not affect the crystal structure. The only difference between these XRD results is that the ZIF-C 85-124 has slightly higher intensity, followed by ZIF-72 and ZIF-C 30-70, indicating its highest crystallinity. $N_2$ adsorption results (**Figure S2**) show that insignificant pores exist inside these ZIF-Cs, indicating ZIF-Cs' non-porous crystal structure similar to that of the leaf-like ZIF-C. The presence of PVA seems to have insignificant influence from this respect.

However, all ZIF-Cs synthesized in PVA solutions display cuboid morphology, different from the leaf-like ZIF-L reported by Wang *et al.*.[46] In addition, all these ZIF-Cs have a similar size compared with their analogue prepared in $H_2O$, except for the different thickness. For example, the dimensions for ZIF-C 30-70 are 5 μm × 2 μm × 70 nm, as listed in **Table S1**, while the leaf-like ZIF-L has the similar length and width (5 μm × 2 μm) but larger thickness (150 nm).[46] Moreover, the length and width of these cuboid ZIF-Cs are negatively related with the molecular weight of the used PVA, even though the same concentration was used. On the other hand, with respect to the thickness, a totally opposite trend is observed that, the longer PVA chain is used in synthesis solution, the thicker the ZIF-Cs are (85-124: 170 nm, 72: 120 nm and 30-70: 70 nm). Moreover, the difference between the thickness of these ZIF-Cs prepared in PVA solution and the one from $H_2O$ (150 nm) is much less. It is speculated that the PVA chains may attach on the surface of small crystals by the interaction between the dangling Zn center[32] and OH groups[33] and inhibit the growth among certain directions, leading to the cuboid 2D morphology. In addition, the results indicate that the shorter PVA chains have the higher possibility to attach on some surfaces of ZIF-C crystals as a result of the higher mobility in solution, generating more inhibition and thus the thinner ZIF-C. To confirm this speculation, XPS tests were conducted and the results are present in **Figure S3-S5**. The main peak in the C 1s spectra of the ZIF-C 3070 has been correlated to the C-C bond at 284.8 eV. The shoulder peak at higher binding energy is assigned to PVA (**Figure S3 (A)**). Significant peak shifts in Zn 2p and N 1s spectra have been observed when comparing with neat ZIF-C, suggesting the formation of coordination bond between Zn and O. Similar behavior has been also reported in the literature for the ZIF-L system.[47] These results indicate the interactions between PVA and ZIF-Cs.

The chemistry of the ZIF-Cs synthesized in PVA solutions are evaluated by FT-IR, and the resultant spectra are shown in **Figure 1 (D)**. Considering the chemical structure of ZIF-Cs, their characteristic peaks are mainly derived by the imidazole ring. For example, the one at 1565 $cm^{-1}$ associates with the vibrations of C=N bond in imidazole ring, as well as the peaks at 1143, 992 $cm^{-1}$ (C-N) and 2925 $cm^{-1}$ (C-H).[48, 49] All these peaks are agreed with the spectrum of the ZIF-L synthesized in $H_2O$. Moreover, a board peak between 3500 – 3100 $cm^{-1}$ and the peaks at 1420 and 1375 $cm^{-1}$ exist in three ZIF-Cs spectra, usually referring to the presence of OH bonds, $CH_2$ blend, and C-H deformation, respectively, which confirms the existence of PVA inside the ZIF-Cs nanosheets- the residue from the synthesis procedure.[50]

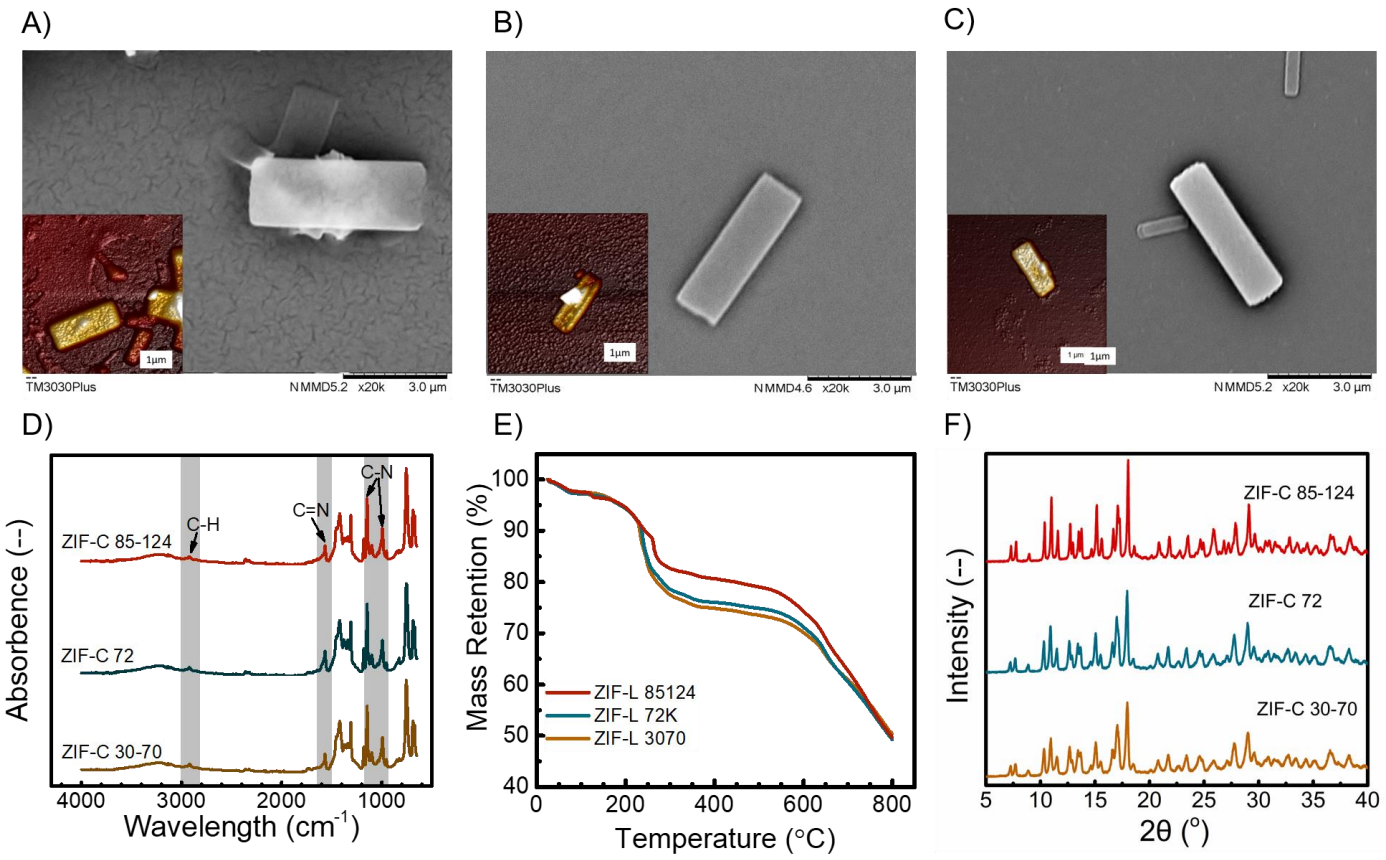


**Figure 1.** The morphology of A) ZIF-C 30-70, B) ZIF-C 72 and C) ZIF-C 85-124 nanosheets, and D) FTIR spectra, E) TGA curves and F) XRD results of ZIF-C nanosheets prepared in PVA solutions

The thermal properties of 2D ZIF-Cs prepared in different PVA solutions are also evaluated by TGA, and the results are shown in **Figure 1 (E)**. As can be seen, all the ZIF-Cs synthesized in PVA solution have similar three-stage decomposition curves. The first one is shown below 100 °C, and only < 3% weight is observed from the weight profiles, which corresponds to the removal of the remaining solvent ($H_2O$). Following a small plateau between 100 and 200 °C, a steep reduction in the weights of these ZIF-Cs occurred at around 220 – 260 °C. The possible reason may be loss of the structural water molecules[37] and the residual PVA. During crystal growth, because of the interaction between zinc ions and the OH groups, PVA polymeric chains may be absorbed on the surface of the developing crystals, then inlaid inside the later growing ZIF-C crystal and change the shape. In addition, it is worth mentioning that the remaining weight of ZIF-Cs at around 220 °C matches with the order of PVA molecular weight (85-124 > 72 > 30-70), indicating longer PVA polymeric chains have less mobility and absorb less onto ZIF-C crystals; hence less PVA is contained in ZIF-C nanosheets. All ZIF-C nanosheets begin to collapse and are carbonized from 500 °C, which fits the profile of ZIF-L crystal reported in the literature.[51-53] These results are also in agreement with the FTIR results.

## PEBAX/ZIF-C MEMBRANE CHARACTERIZATION

For mixed matrix membranes, the interfacial relationship between the polymeric matrix and inorganic fillers is crucial for the overall performance.[2] For example, the poor interface between fillers and polymeric chains may cause nanoscale interface voids, further causing the lower transport resistance and low or even non-selectivity in the membrane. Inorganic fillers, especially nano-fillers, may be more easily aggregated, which also leads to the formation of pinholes inside the membrane, thus resulting in the deteriorated selectivity.

The surface and cross-section SEM images of MMMs with various ZIF-C 85-124 loading are present in **Figure 2 (A-D)**. The neat Pebax membranes have smooth, defect-free surface and cross-section, as expected. For the ones containing ZIF-C 85-124 of up to 20 wt.%, the ZIF-C 85-124 is uniformly dispersed in the membrane without noticeable agglomeration. Similar morphology of MMMs with the other ZIF-Cs were also observed from SEM, as shown in **Figure S6** and **Figure S7**. These images demonstrate the good polymer-filler contact between the ZIF-C prepared from PVA solution and Pebax matrix, which may be attributed by the PVA chains around ZIF-Cs. The influence of different ZIF-C on the morphology of MMMs was also investigated, as shown in **Figure 2 (D-E)**. The membrane contained ZIF-C 30-70 has the smallest nanofillers, while

the fillers in MMMs with ZIF-C 85-124 has the biggest size among these three, which matched the morphology of ZIF-Cs. Moreover, these three ZIF-Cs are generally uniformly distributed on the surface and cross-section of MMMs with a loading of 20 wt. %. However, some ZIF-C 30-70 sheets are observed to be stacked from the cross-section, due probably to the aggregation tendency of these thin nanosheets.

The chemistry nature of these MMMs with different ZIF-Cs is studied by FT-IR. The typical peaks of neat polymer (3303 $cm^{-1}$ for N-H, 2871 $cm^{-1}$ for C-H, 1731 $cm^{-1}$ for C=P, 1638 $cm^{-1}$ for –C=O and 1095 $cm^{-1}$ for C-O) are apparent in the spectrum of Pebax membrane, as evidenced in **Figure S8 (C)**, which is in accordance with its chemical structure and the peaks reported in the literature.[35] With the increasing ZIF-C 85-124 content, the intensities of these peaks decrease while those from ZIF-Cs, like C-N bond in imidazole ring (1143 $cm^{-1}$ and 992 $cm^{-1}$), become more and more significant in the FTIR curves, as present in **Figure 3 (A)**, indicating that the content of ZIF-Cs 85-124 inside MMMs increases as expected. The other MMMs containing ZIF-C 72 or ZIF-30-70 have a similar trend with the addition of ZIF-C nano-sheets and the spectra are presented in **Figure S8**. Meanwhile, no peaks have been generated or disappeared in the spectra of MMMs compared with those of the neat polymer or the ZIF-Cs; hence we conclude there is no chemical reaction between ZIF-C 85-124 and the Pebax polymeric matrix. The ZIF-C nano-sheets are physically embedded into the Pebax polymeric matrix. For the MMMs containing different ZIF-Cs with the same loading, their spectra are found to be almost identical, demonstrating the chemical similarity of these ZIF-C nano-sheets and thus the resultant MMMs, as shown in **Figure 3 (D)**.

The thermal stability of MMMs containing ZIF-C nano-sheets has been investigated by TGA. The neat polymer starts decomposed around 330 °C with a single-stage behavior, which is higher than that of ZIF-Cs. As a result, the thermal stability of MMMs deteriorates with the increasing content of ZIF-Cs, as shown in **Figures 3 (B)** and **Figure S9**. For the MMMs with 5% ZIF-C 85-124, the $T_{onset}$ is still higher than 300 °C, but the value for MMMs with 20% ZIF-C decreases to around 200 °C with only 4% loss at this stage. From these results, the addition of ZIF-C into Pebax matrix is also confirmed, agreed with the FTIR results. However, most of the membranes for post-combustion $CO_2$ capture are operated at a temperature lower than 80 °C, depending on the process. Therefore, these membranes are still qualified in terms of thermal stability. For the membranes containing different ZIF-Cs, their thermal stabilities are very similar, as shown in **Figure 3 (E)**. The only difference is the slightly lower weight loss between 200 and 300 °C in the one with ZIF-C 85-124 because of the marginally better thermal stability of ZIF-C 85-124 compared with the other ZIF-Cs.

The crystallinity analysis of the MMMs was also conducted by XRD, as shown in **Figure 3(C), (F)** and **Figure S10**. The XRD pattern of Pebax displays an amorphous structure, as expected, with the broad pattern shape from 9° to 27°. From **Figure 3(C)**, it is clearly observed that the incorporation of ZIF-C 85-124 into MMMs introduces sharp peaks into the broad curve of the neat polymer. These peaks become clearer with the increasing ZIF-C loading. A similar trend is also observed for MMMs with different ZIF-Cs. The one with ZIF-C 85-124 has slightly sharper ZIF-C peaks compared with the MMMs containing the other ZIF-Cs because of the higher intensity of ZIF-C 85-124.

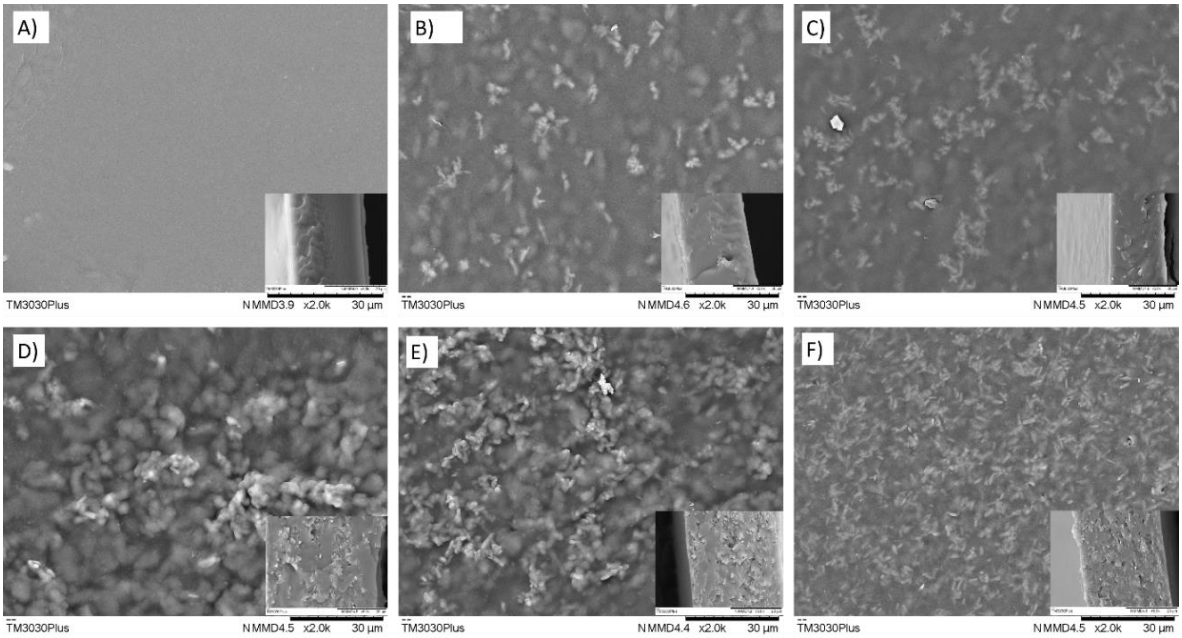


**Figure 2.** Morphology of MMMs with A) 0%, B) 5%, C) 10% and D) 20% ZIF-C 85-124, E) 20% ZIF-C 72 and F) 20% ZIF-C 30-70.

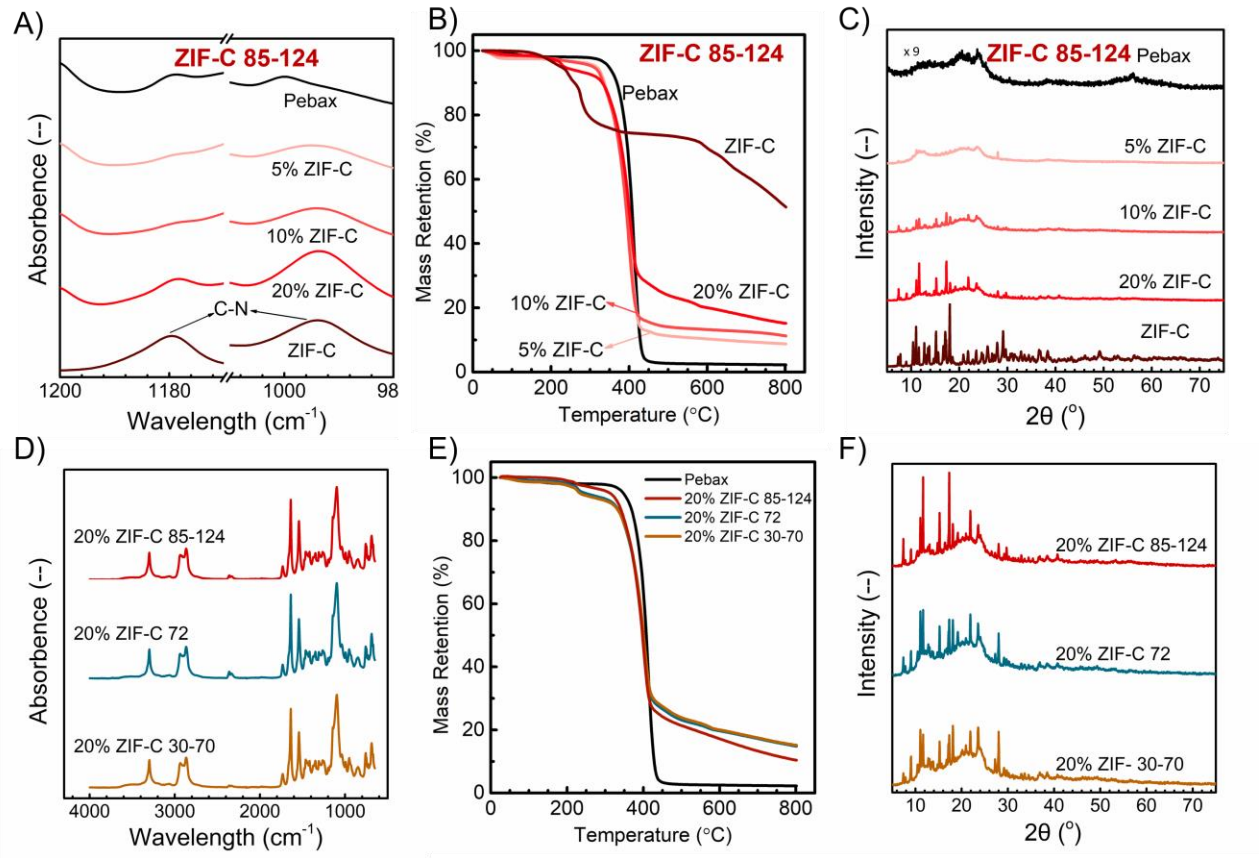


**Figure 3.** The A) FTIR spectra, B) TGA curves and C) XRD results of Pebax +ZIF-C 85-124 MMMs with different ZIF-C content, and D) FTIR spectra, E) TGA curves and F) XRD results of MMMs with 20% different ZIF-C nanosheets. The scale of Pebax' XRD results are 9 times smaller than the others.

## GAS PERMEATION PROPERTIES

The mixed gas permeation tests are conducted to study the effects of different ZIF-C nanosheets on the $CO_2$ separation performance of Pebax + ZIF-C MMMs. As shown in **Figure 4**, the $CO_2$ permeability ($P(CO_2)$) of neat Pebax 1657 membrane under dry condition is 71.3 Barrer with a $CO_2/N_2$ selectivity of around 30, which is in agreement with the literature value.[35] Regardless of the different morphologies, the addition of these ZIF-C nanosheets increases the $P(CO_2)$ and $CO_2/N_2$ separation factor of MMMs under dry condition within ZIF-Cs contents of up to 10 wt.%. The $CO_2$ permeability of MMMs with 10 wt.% ZIF-C 85-124 is found to be 141.7 Barrer, almost twice of value from the neat Pebax membrane, with a slightly enhanced $CO_2/N_2$ selectivity of 32.8. These results may be explained from several aspects. Firstly, the interlayer channels inside ZIF-C endows a fast transportation shortcut for $CO_2$ and therefore benefits the $CO_2$ permeability.[54] Meanwhile, for $N_2$, the presence of ZIF-C rigidifies the polymer chains[55, 56] and increases tortuosity and thus the transport pathway for gases, leading to enhanced $CO_2/N_2$ selectivity. In addition, the increment in $CO_2/N_2$ selectivity implies the absence of interface voids between polymer and filler phases at low ZIF-C loading.[6] However, the existence of interface voids was observed with further addition of ZIF-C,[57] as the result of the decreased $CO_2$ permeability and $CO_2/N_2$ in all MMMs. In the case of $CO_2$ permeability, the contribution of this pathway counteracts the benefit from the selective sorption of ZIF-Cs, causing a slight loss in $CO_2$ permeability rather than a further increment.

In addition to the nanofiller loading, the morphology of these ZIF-C nanosheets also affects the final performances of MMMs. It has been reported that for fillers with a high aspect ratio, like the ones used in this work, the nanoscale dimension plays a much greater role in the material properties of the neat fillers and the resultant MMMs. [18, 20, 30] Considering the relatively smaller changes in the length and width of these ZIF-Cs than in thickness, and only the thicknesses are in nanoscale, the morphology effects discussed here are only related to the changes in thickness. The membranes with ZIF-C 85-124 show the highest $CO_2$ permeability within all studied filler contents in this work, followed by ZIF-C 30-70 and ZIF-C 72, while the selectivities show a reverse order. The highest improvement in $CO_2$ permeability may be explained by the greater effects of the selective $CO_2$ adsorption of thicker ZIF-C nanosheets due to the more available pathway for gases between layers. Moreover, the membranes containing thicker 2D nanosheets may have lower tortuosity and thus lower gas transport resistance, leading to higher gas permeability. On the other hand, lower tortuosity

is usually less favorable to the selectivity, so as the relative lower $CO_2/N_2$ selectivity of MMMs with ZIF-C 85-124 compared to the other membranes. These trends match the results of the Pebax+ZIF-72 membranes, in which the higher tortuosity caused by the thinner ZIF-C leads to less increment in the gas permeability but higher $CO_2/N_2$ selectivity. However, for the MMMs containing thinnest ZIF-C 30-70, the lower $CO_2$ permeability and the lower $CO_2/N_2$ selectivity may be ascribed to the stacked nanosheets inside MMMs, as observed from SEM images, leading to the less selective voids between nanosheets.

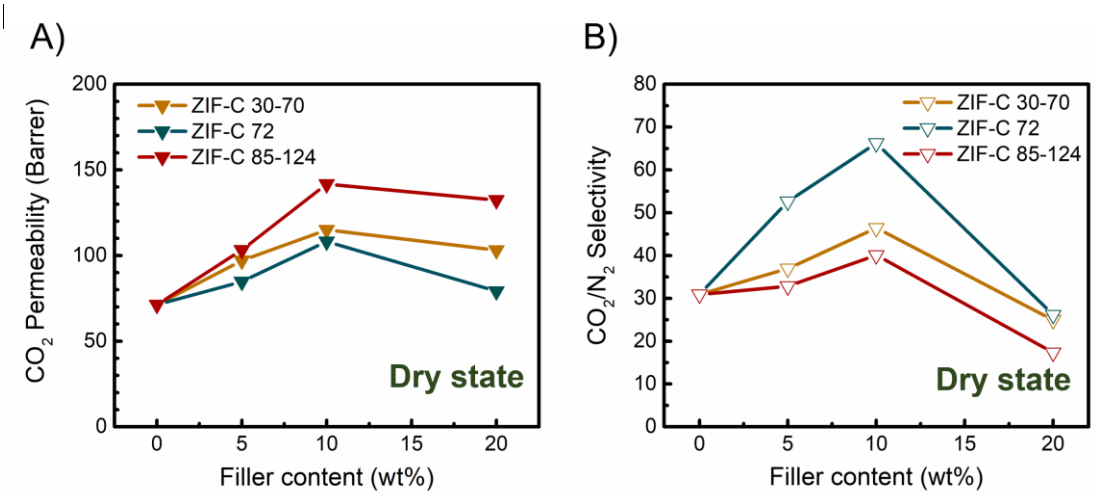


**Figure 4.** The (A) $CO_2$ permeability and (B) $CO_2/N_2$ selectivity of Pebax + ZIF-C MMMs as a function of filler content at the dry state.

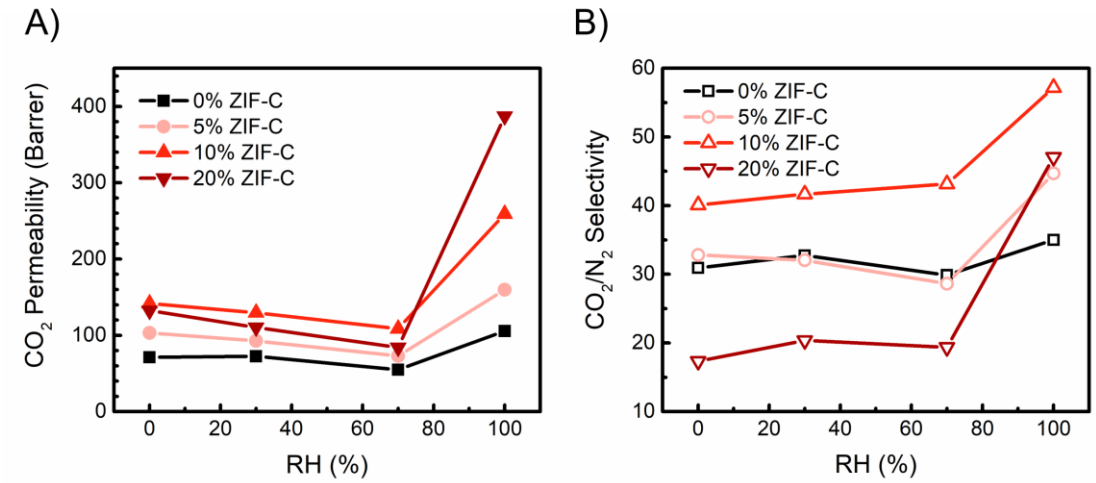


**Figure 5.** (A) $CO_2$ permeability and (B) $CO_2/N_2$ selectivity of Pebax + ZIF-C 85-124 MMMs as a function of RH.

As a hydrophilic material, the gas separation performance of Pebax is affected by the relative humidity of the tested gases. [35, 58, 59] The $CO_2$ permeability of the neat Pebax membrane (71.3 Barrer at dry condition) decreases (54.7 Barrer at 70 RH%) and then increases with the increasing relative humidity (105.6 Barrer at 100 RH%), and a similar trend is also observed for $CO_2/N_2$ selectivity, as shown in **Figure 5**. Water vapor first occupies the original free volume, leading to the decreased gas permeability and then swells Pebax polymeric chains, resulting in enhanced gas flux. The fully swollen polymer matrix also benefits the solubility and diffusivity of $CO_2$, thereby obtaining the simultaneous increment in $CO_2$ permeability and $CO_2/N_2$ selectivity. [58, 60] This trend is also observed in MMMs containing ZIF-Cs nanosheets, as presented in **Figure 5**. For instance, the Pebax + 10% ZIF-C 85-124 membrane has a $CO_2$ permeability of 141.7 Barrer with a selectivity of 40.1 at dry condition. With humidity increasing to 70 RH%, the $CO_2$ permeability decreases to 108.6 Barrer. However, further humidification from 70 RH% to 100 RH% leads to an around 2-fold increment in $CO_2$ permeability (259.2 Barrer) and the $CO_2/N_2$ selectivity (57.2). Apart from the benefits as mentioned, the rigidification of Pebax chains around ZIF-C MMMs could be eased due to the increased flexibility of polymeric chains at the swollen state. However, despite the low $CO_2$ permeability and $CO_2/N_2$ selectivity under dry conditions, the membrane with 20% ZIF-C 85-124 has the most significant increase in $CO_2$ permeability (4.6-flod, 387.2 Barrer) and $CO_2/N_2$ selectivity (2.4-fold, 47.1) when the separated gas is fully saturated with water vapor. The increased performance is because that the swollen Pebax chains expand and fill the interfacial voids between polymeric matric and ZIF-C nanosheets,

which reduces the nonselective elements and increases the selectivity. In addition to the benefit from humidified membranes, the selective adsorption via ZIF-Cs also benefits the $CO_2$ permeation, while the transportation of $N_2$ only depends on the solution-diffusion mechanism. Similar results are obtained for MMMs with ZIF-C 30-70 and ZIF-C 72, as shown in **Figure S11** and **S12**.

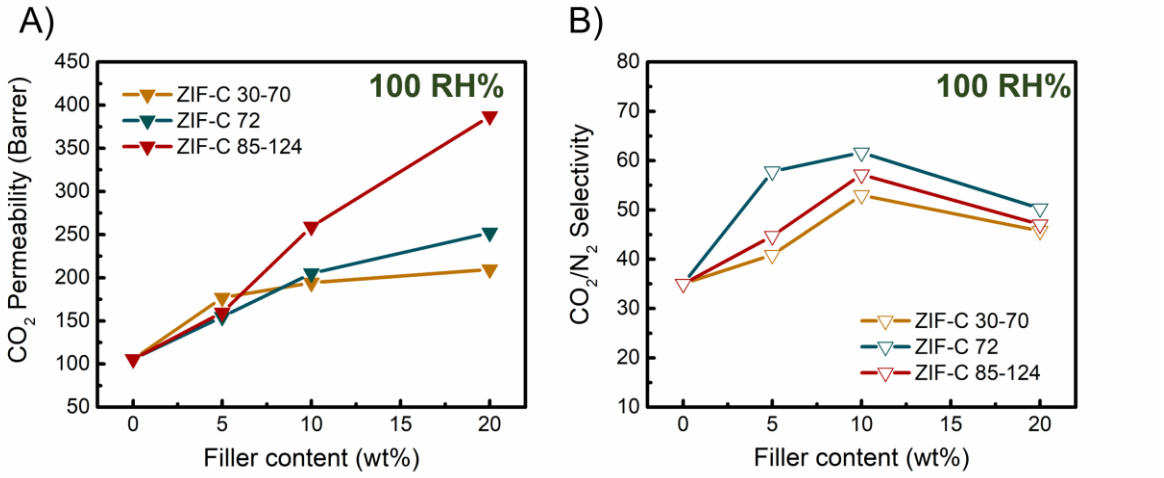


**Figure 6.** The (A) $CO_2$ permeability and (B) $CO_2/N_2$ selectivity of Pebax + ZIF-C MMMs as a function of filler content at 100 RH%

Therefore, under the fully water vapor saturated condition, $CO_2$ separation performance of the Pebax + ZIF-Cs nanosheets has different behavior compared with that under the dry condition. Increment has been observed in both $CO_2$ permeability and selectivity for all MMMs as shown in **Figure 6**. The influence of morphology for $CO_2$ separation performance under the fully water vapor saturated condition is quite similar to that under the dry condition. As discussed above, the membranes containing ZIF-C 72 have relatively higher tortuosity compared to the other analogies and thus display the highest $CO_2/N_2$ selectivity and relatively low gas permeability under dry condition. The same trend has also been observed in the results under fully humid condition. But due to the presence of more stacked nanosheets, the MMMs with ZIF-C 30-70 display the lowest $CO_2$ permeability and $CO_2/N_2$ selectivity when the ZIF-C nanosheet loading is higher than 5 wt. % even though they are the median under the dry condition.

These performances are evaluated in comparison with the 2008 Robeson bound,[5] as shown in **Figure 7**, and some Pebax 1657-based MMMs in the literature, [1-3, 27, 35, 61-70] as presented in **Table 1**. It is clearly seen that the incorporation of ZIF-C 85-124 pushes the performance close to the upper bound with the loading of up to 10 wt.%, and then move along the upper bound with the higher ZIF-C loading. In addition, it is clearly shown that the addition of ZIF-Cs into Pebax greatly improved both $CO_2$ permeability and $CO_2/N_2$ selectivity.

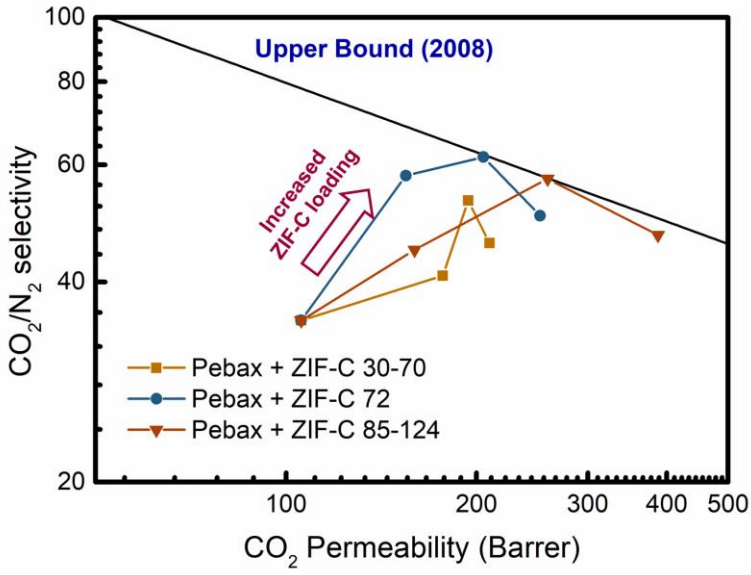


**Figure 7.** $CO_2/N_2$ separation performances of Pebax 1657-based MMMs at 100% RH condition separation.

**Table 1** The start-of-art of the $CO_2/N_2$ performance of the Pebax 1657-based MMMs

| Fillers | $P(CO_2)$ / Barrer | $CO_2/N_2$ selectivity | Tested condition | Ref |
|---|---|---|---|---|
| Zeolite-4A[a] | 129.5 | 94.2 | Single gas, 24.5 Bar, R.T. | 62 |
| Fumed silica | 74.12 | 101.53 | Mixed gas, 12 Bar, 25 °C | 70 |
| ZIF-8 (90 nm) | 99.7 | 59.6 | Single gas, 1 Bar, 20 °C | 27 |
| MIL-53 | 95.7 | 49.9 | Single gas, 10 Bar, 35 °C | 68 |
| Attapulgite | ~ 180 | 52 | Humid single gas, 35 °C | 67 |
| | ~ 250 GPU | ~ 70 | Humid mixed gas, 35 °C (25 vol% $CO_2$ in $N_2$) | 71 |
| PEG-g-CNT | 369.1 | 110.8 | Humid mixed gas, 2 Bar, 24 °C | 35 |
| Graphene oxide (GO) | 100 | 91 | Single gas, 3 Bar, 25 °C | 72 |
| Porous reduced GO | 119 | 104 | Single gas, 2 Bar, 30 °C | 65 |
| Imidazole GO | 76.2 | 105 | Single gas, 8 Bar, 25 °C | 66 |
| $MoS_2$ | 64 | 93 | Single gas, 2 Bar, 30 °C | 73 |
| Multi-walled carbon nanotubes (MWCNTs) | 361 | 52 | Single gas, 7 Bar, 35 °C | 63 |
| MWCNTs | 262.2 | 58.5 | Single gas, 1 Bar, R.T. | 61 |
| ZIF-C 85-124 | 387.2 | 47.1 | Humid mixed gas, 2 Bar, 24 °C | This work |
| ZIF-C 72k | 205.1 | 61.6 | | |
| ZIF-C 30-70 | 194.2 | 53.0 | | |

## CONCLUSIONS

In this work, a simple preparation method for cuboid ZIF-C nanosheets with controllable morphology has been developed. Three PVA with different molecular weights were employed to investigate its effect on the morphology of the nanosheets. The results show that the molecular weight of the additive PVA has a significant influence on the thickness and size of the as-synthesized ZIF-C nanosheets, as well as the material properties. The higher MW the PVA has, the thicker and smaller in both length and width the ZIF-C nanosheets are formed. The crystal structure of the ZIF-C is proven by the $N_2$ adsorption experiment and XRD tests. During the growth of crystals, PVA chains are selectively attached to some surfaces of the crystals and inhibit the growth along with the particular directions. Thus, the shape and the size of these nanosheets can be manipulated. The existence of PVA inside the ZIF-C nanosheets is confirmed by FTIR and TGA analysis. In addition, the one made from PVA 85-124 solution has the best thermal stability and highest crystallinity among the as-synthesized ZIF-C nanosheets.

With the Pebax 1657 as the polymeric matrix, the effect of these ZIF-C nanosheets in mixed matrix membranes has been systemically studied by various techniques. The results from FTIR, XRD, and TGA tests confirm the successful incorporation of the ZIF-C nanosheets into the Pebax phase. The surface and cross-section images from SEM analysis show that these nanosheets are generally well-dispersed in the MMMs. However, stacked ZIF-C 30-70s, the thinnest nanosheet obtained in this work, are noticeable from SEM images. Moreover, the mixed gas permeation results show that the addition of the ZIF-C nanosheets increases the permeability and $CO_2/N_2$ selectivity, regardless of the kind or the content of the nanosheets. ZIF-C 85-124, the thickest nanosheet prepared in this work, is found to be the most efficient nanofiller in promoting $CO_2$ transport compared with the others because of the selective adsorption of $CO_2$ inside the ZIF-C nanosheets. Furthermore, the presence of water vapor significantly enhances the gas transport property, and the $CO_2$ separation efficiency of these MMMs. The highest $CO_2$ permeability (387.2 Barrer) with a $CO_2/N_2$ selectivity of 47.1 is obtained from the Pebax + 20% ZIF-C 85-124 MMM.

Overall, this method provides a facile approach to the fabrication of ZIF-C nanosheets with controllable size and thickness. The as-synthesized ZIF-C nanosheets can be used as promising nano-fillers in MMMs to enhance $CO_2$ separation performance. The preparation methods reported here may be further studied by using different additives to form other shapes of nanoparticles, or to better understand the effect of the additives on the crystal formation and growth, and the morphology of the nanoparticles. Other polymers may also be applied as the membrane polymer phases for MMMs with even better $CO_2$ separation performance or for different applications.

## ASSOCIATED CONTENT

### Supporting Information

The Supporting Information is available free of charge on the ACS Publications website.

The size and the curves obtained from $N_2$ absorption, XPS results of the as-synthesized ZIF-C; FTIR spectra, TGA curves, XRD results and the permeation results of the MMMs containing ZIF-C 72 and ZIF-C 30-70.

## AUTHOR INFORMATION

**Corresponding Author**

Liyuan Deng

Email: deng@nt.ntnu.no

**ORCID**

Jing Deng: 0000-0003-3680-3799

Zhongde Dai: 0000-0002-3558-5403

Liyuan Deng: 0000-0003-4785-4620

**Author Contributions**

The manuscript was written through the contributions of all authors. All authors have given approval to the final version of the manuscript.

**Funding Sources**

This work is supported by the Research Council of Norway through the CLIMIT program ("POLYMEM" project, No. 254791).

**Notes**

There are no conflicts to declare.

## ACKNOWLEDGMENT

This work is supported by the Research Council of Norway through the CLIMIT program ("POLYMEM" project, No. 254791). The authors highly acknowledge Dr. Yizhi Zhuo (Department of Structural Engineering, NTNU) and Dr. Weixin Qian (School of Chemical Engineering, East China University of Science and Technology) for their kind help in the AFM and BET characterization.

## REFERENCES

1. Seoane, B.; Coronas, J.; Gascon, I.; Etxeberria Benavides, M.; Karvan, O.; Caro, J.; Kapteijn, F.; Gascon, J., Metal-organic framework based mixed matrix membranes: a solution for highly efficient $CO_2$ capture? *Chem. Soc. Rev.* **2015,** 44, (8), 2421-54.
2. Chung, T.-S.; Jiang, L. Y.; Li, Y.; Kulprathipanja, S., Mixed matrix membranes (MMMs) comprising organic polymers with dispersed inorganic fillers for gas separation. *Prog. Polym. Sci.* **2007,** 32, (4), 483-507.
3. Kang, Z.; Fan, L.; Sun, D., Recent advances and challenges of metal–organic framework membranes for gas separation. *J. Mater. Chem. A* **2017,** 5, (21), 10073-10091.
4. Moghadam, P. Z.; Li, A.; Wiggin, S. B.; Tao, A.; Maloney, A. G. P.; Wood, P. A.; Ward, S. C.; Fairen-Jimenez, D., Development of a Cambridge Structural Database Subset: A Collection of Metal–Organic Frameworks for Past, Present, and Future. *Chem. Mater.* **2017,** 29, (7), 2618-2625.
5. Robeson, L. M., The upper bound revisited. *J. Membr. Sci.* **2008,** 320, (1-2), 390-400.
6. Park, H. B.; Kamcev, J.; Robeson, L. M.; Elimelech, M.; Freeman, B. D., Maximizing the right stuff: The trade-off between membrane permeability and selectivity. *Science* **2017,** 356, (6343), eaab0530.
7. Liu, M.; Gurr, P. A.; Fu, Q.; Webley, P. A.; Qiao, G. G., Two-dimensional nanosheet-based gas separation membranes. *J. Mater. Chem. A* **2018,** 6, (46), 23169-23196.
8. Lin, R.; Villacorta Hernandez, B.; Ge, L.; Zhu, Z., Metal organic framework based mixed matrix membranes: an overview on filler/polymer interfaces. *J. Mater. Chem. A* **2018,** 6, (2), 293-312.
9. Mon, M.; Bruno, R.; Tiburcio, E.; Grau-Atienza, A.; Sepúlveda-Escribano, A.; Ramos-Fernandez, E. V.; Fuoco, A.; Esposito, E.; Monteleone, M.; Jansen, J. C.; Cano, J.; Ferrando-Soria, J.; Armentano, D.; Pardo, E., Efficient Gas Separation and Transport Mechanism in Rare Hemilabile Metal–Organic Framework. *Chem. Mater.* **2019,** 31, (15), 5856-5866.
10. Bux, H.; Feldhoff, A.; Cravillon, J.; Wiebcke, M.; Li, Y.-S.; Caro, J., Oriented Zeolitic Imidazolate Framework-8 Membrane with Sharp $H_2/C_3H_8$ Molecular Sieve Separation. *Chem. Mater.* **2011,** 23, (8), 2262-2269.
11. Chen, S.; Lucier, B. E. G.; Boyle, P. D.; Huang, Y., Understanding The Fascinating Origins of $CO_2$ Adsorption and Dynamics in MOFs. *Chem. Mater.* **2016,** 28, (16), 5829-5846.
12. Anderson, R.; Rodgers, J.; Argueta, E.; Biong, A.; Gómez-Gualdrón, D. A., Role of Pore Chemistry and Topology in the $CO_2$ Capture Capabilities of MOFs: From Molecular Simulation to Machine Learning. *Chem. Mater.* **2018,** 30, (18), 6325-6337.
13. Bien, C. E.; Liu, Q.; Wade, C. R., Assessing the Role of Metal Identity on $CO_2$ Adsorption in MOFs Containing M–OH Functional Groups. *Chem. Mater.* **2019,** 32, (1), 489-497.
14. Hess, S. C.; Grass, R. N.; Stark, W. J., MOF Channels within Porous Polymer Film: Flexible, Self-Supporting ZIF-8 Poly(ether sulfone) Composite Membrane. *Chem. Mater.* **2016,** 28, (21), 7638-7644.
15. Dechnik, J.; Gascon, J.; Doonan, C. J.; Janiak, C.; Sumby, C. J., Mixed-Matrix Membranes. *Angew. Chem. Int. Ed.* **2017,** 56, (32), 9292-9310.
16. Bae, T.-H.; Lee, J. S.; Qiu, W.; Koros, W. J.; Jones, C. W.; Nair, S., A High-Performance Gas-Separation Membrane Containing Submicrometer-Sized Metal–Organic Framework Crystals. *Angew. Chem. Int. Ed.* **2010,** 49, (51), 9863-9866.
17. Hwang, S.; Chi, W. S.; Lee, S. J.; Im, S. H.; Kim, J. H.; Kim, J., Hollow ZIF-8 nanoparticles improve the permeability of mixed matrix membranes for $CO_2/CH_4$ gas separation. *J. Membr. Sci.* **2015,** 480, 11-19.
18. Rodenas, T.; Luz, I.; Prieto, G.; Seoane, B.; Miro, H.; Corma, A.; Kapteijn, F.; Llabrés i Xamena, F. X.; Gascon, J., Metal–organic framework nanosheets in polymer composite materials for gas separation. *Nature Materials* **2014,** 14, 48.
19. Sabetghadam, A.; Seoane, B.; Keskin, D.; Duim, N.; Rodenas, T.; Shahid, S.; Sorribas, S.; Le Guillouzer, C.; Clet, G.; Tellez, C.; Daturi, M.; Coronas, J.; Kapteijn, F.; Gascon, J., Metal Organic Framework Crystals in Mixed-Matrix Membranes: Impact of the Filler Morphology on the Gas Separation Performance. *Adv. Funct. Mater.* **2016,** 26, (18), 3154-3163.
20. Kang, Z.; Peng, Y.; Hu, Z.; Qian, Y.; Chi, C.; Yeo, L. Y.; Tee, L.; Zhao, D., Mixed matrix membranes composed of two-dimensional metal–organic framework nanosheets for pre-combustion $CO_2$ capture: a relationship study of filler morphology versus membrane performance. *J. Mater. Chem. A* **2015,** 3, (41), 20801-20810.
21. Galizia, M.; Chi, W. S.; Smith, Z. P.; Merkel, T. C.; Baker, R. W.; Freeman, B. D., 50th Anniversary Perspective: Polymers and Mixed Matrix Membranes for Gas and Vapor Separation: A Review and Prospective Opportunities. *Macromolecules* **2017,** 50, (20), 7809-7843.
22. Jeong, H.-K.; Krych, W.; Ramanan, H.; Nair, S.; Marand, E.; Tsapatsis, M., Fabrication of Polymer/Selective-Flake Nanocomposite Membranes and Their Use in Gas Separation. *Chem. Mater.* **2004,** 16, (20), 3838-3845.
23. Ahmadi, M.; Janakiram, S.; Dai, Z.; Ansaloni, L.; Deng, L., Performance of mixed matrix membranes containing porous two-dimensional (2D) and three-dimensional (3D) fillers for $CO_2$ separation: a review. *Membranes* **2018,** 8, (3), 50.
24. Janakiram, S.; Ahmadi, M.; Dai, Z.; Ansaloni, L.; Deng, L., Performance of nanocomposite membranes containing 0D to 2D nanofillers for $CO_2$ separation: A review. *Membranes* **2018,** 8, (2), 24.
25. Japip, S.; Xiao, Y.; Chung, T.-S., Particle-Size Effects on Gas Transport Properties of 6FDA-Durene/ZIF-71 Mixed Matrix Membranes. *Ind. Eng. Chem. Res.* **2016,** 55, (35), 9507-9517.

26. Sánchez-Laínez, J.; Zornoza, B.; Friebe, S.; Caro, J.; Cao, S.; Sabetghadam, A.; Seoane, B.; Gascon, J.; Kapteijn, F.; Le Guillouzer, C.; Clet, G.; Daturi, M.; Téllez, C.; Coronas, J., Influence of ZIF-8 particle size in the performance of polybenzimidazole mixed matrix membranes for pre-combustion $CO_2$ capture and its validation through interlaboratory test. *J. Membr. Sci.* **2016,** 515, 45-53.

27. Zheng, W.; Ding, R.; Yang, K.; Dai, Y.; Yan, X.; He, G., ZIF-8 nanoparticles with tunable size for enhanced $CO_2$ capture of Pebax based MMMs. *Sep. Purif. Technol.* **2019,** 214, 111-119.

28. Knebel, A.; Friebe, S.; Bigall, N. C.; Benzaqui, M.; Serre, C.; Caro, J., Comparative Study of MIL-96(Al) as Continuous Metal–Organic Frameworks Layer and Mixed-Matrix Membrane. *ACS Appl. Mater. Interfaces* **2016,** 8, (11), 7536-7544.

29. Zhao, M.; Huang, Y.; Peng, Y.; Huang, Z.; Ma, Q.; Zhang, H., Two-dimensional metal–organic framework nanosheets: synthesis and applications. *Chem. Soc. Rev.* **2018,** 47, (16), 6267-6295.

30. Johnson, J. R.; Koros, W. J., Utilization of nanoplatelets in organic–inorganic hybrid separation materials: Separation advantages and formation challenges. *Journal of the Taiwan Institute of Chemical Engineers* **2009,** 40, (3), 268-275.

31. Kim, S.; Shamsaei, E.; Lin, X.; Hu, Y.; Simon, G. P.; Seong, J. G.; Kim, J. S.; Lee, W. H.; Lee, Y. M.; Wang, H., The enhanced hydrogen separation performance of mixed matrix membranes by incorporation of two-dimensional ZIF-L into polyimide containing hydroxyl group. *J. Membr. Sci.* **2018,** 549, 260-266.

32. Yang, Y.; Goh, K.; Wang, R.; Bae, T.-H., High-performance nanocomposite membranes realized by efficient molecular sieving with CuBDC nanosheets. *Chem. Commun.* **2017,** 53, (30), 4254-4257.

33. Shete, M.; Kumar, P.; Bachman, J. E.; Ma, X.; Smith, Z. P.; Xu, W.; Mkhoyan, K. A.; Long, J. R.; Tsapatsis, M., On the direct synthesis of Cu(BDC) MOF nanosheets and their performance in mixed matrix membranes. *J. Membr. Sci.* **2018,** 549, 312-320.

34. Cheng, Y.; Tavares, S. R.; Doherty, C. M.; Ying, Y.; Sarnello, E.; Maurin, G.; Hill, M. R.; Li, T.; Zhao, D., Enhanced Polymer Crystallinity in Mixed-Matrix Membranes Induced by Metal–Organic Framework Nanosheets for Efficient $CO_2$ Capture. *ACS Appl. Mater. Interfaces* **2018,** 10, (49), 43095-43103.

35. Dai, Z.; Deng, J.; Peng, K.-J.; Liu, Y.-L.; Deng, L., Pebax/PEG Grafted CNT Hybrid Membranes for Enhanced $CO_2/N_2$ Separation. *Ind. Eng. Chem. Res.* **2019,** 58, (27), 12226-12234.

36. Dai, Z.; Aboukeila, H.; Ansaloni, L.; Deng, J.; Giacinti Baschetti, M.; Deng, L., Nafion/PEG hybrid membrane for $CO_2$ separation: Effect of PEG on membrane micro-structure and performance. *Sep. Purif. Technol.* **2019,** 214, 67-77.

37. Lo, Y.; Lam, C. H.; Chang, C.-W.; Yang, A.-C.; Kang, D.-Y., Polymorphism/pseudopolymorphism of metal–organic frameworks composed of zinc(ii) and 2-methylimidazole: synthesis, stability, and application in gas storage. *RSC Advances* **2016,** 6, (92), 89148-89156.

38. Yang, F.; Mu, H.; Wang, C.; Xiang, L.; Yao, K. X.; Liu, L.; Yang, Y.; Han, Y.; Li, Y.; Pan, Y., Morphological Map of ZIF-8 Crystals with Five Distinctive Shapes: Feature of Filler in Mixed-Matrix Membranes on $C_3H_6/C_3H_8$ Separation. *Chem. Mater.* **2018,** 30, (10), 3467-3473.

39. Pan, Y.; Heryadi, D.; Zhou, F.; Zhao, L.; Lestari, G.; Su, H.; Lai, Z., Tuning the crystal morphology and size of zeolitic imidazolate framework-8 in aqueous solution by surfactants. *CrystEngComm* **2011,** 13, (23).

40. Yao, J.; He, M.; Wang, H., Strategies for controlling crystal structure and reducing usage of organic ligand and solvents in the synthesis of zeolitic imidazolate frameworks. *CrystEngComm* **2015,** 17, (27), 4970-4976.

41. Zheng, G.; Chen, Z.; Sentosun, K.; Pérez-Juste, I.; Bals, S.; Liz-Marzán, L. M.; Pastoriza-Santos, I.; Pérez-Juste, J.; Hong, M., Shape control in ZIF-8 nanocrystals and metal nanoparticles@ZIF-8 heterostructures. *Nanoscale* **2017,** 9, (43), 16645-16651.

42. Fu, H.; Wang, Z.; Wang, X.; Wang, P.; Wang, C.-C., Formation mechanism of rod-like ZIF-L and fast phase transformation from ZIF-L to ZIF-8 with morphology changes controlled by polyvinylpyrrolidone and ethanol. *CrystEngComm* **2018,** 20, (11), 1473-1477.

43. Porel, S.; Singh, S.; Radhakrishnan, T. P., Polygonal gold nanoplates in a polymer matrix. *Chem. Commun.* **2005**, (18), 2387-2389.

44. Sang, W.; Fang, Y.; Fan, J.; He, Y.; Min, J.; Qian, Y., Novel synthesis method of ZnO nanorods by ion complex transformed PVA-assisted nucleation. *J. Cryst. Growth* **2007,** 299, (2), 272-276.

45. Tao, A. R.; Habas, S.; Yang, P., Shape Control of Colloidal Metal Nanocrystals. *Small* **2008,** 4, (3), 310-325.

46. Chen, R.; Yao, J.; Gu, Q.; Smeets, S.; Baerlocher, C.; Gu, H.; Zhu, D.; Morris, W.; Yaghi, O. M.; Wang, H., A two-dimensional zeolitic imidazolate framework with a cushion-shaped cavity for $CO_2$ adsorption. *Chem. Commun.* **2013,** 49, (82), 9500-2.

47. Gao, S.; Hou, J.; Deng, Z.; Wang, T.; Beyer, S.; Buzanich, A. G.; Richardson, J. J.; Rawal, A.; Seidel, R.; Zulkifli, M. Y.; Li, W.; Bennett, T. D.; Cheetham, A. K.; Liang, K.; Chen, V., Improving the Acidic Stability of Zeolitic Imidazolate Frameworks by Biofunctional Molecules. *Chem* **2019,** 5, (6), 1597-1608.

48. Tian, Z.; Yao, X.; Ma, K.; Niu, X.; Grothe, J.; Xu, Q.; Liu, L.; Kaskel, S.; Zhu, Y., Metal–Organic Framework/Graphene Quantum Dot Nanoparticles Used for Synergistic Chemo- and Photothermal Therapy. *ACS Omega* **2017,** 2, (3), 1249-1258.

49. Wu, C.; Liu, Q.; Chen, R.; Liu, J.; Zhang, H.; Li, R.; Takahashi, K.; Liu, P.; Wang, J., Fabrication of ZIF-8@$SiO_2$ Micro/Nano Hierarchical Superhydrophobic Surface on AZ31 Magnesium Alloy with Impressive Corrosion Resistance and Abrasion Resistance. *ACS Appl. Mater. Interfaces* **2017,** 9, (12), 11106-11115.

50. Dai, Z.; Deng, J.; Yu, Q.; Helberg, R. M. L.; Janakiram, S.; Ansaloni, L.; Deng, L., Fabrication and Evaluation of Bio-Based Nanocomposite TFC Hollow Fiber Membranes for Enhanced $CO_2$ Capture. *ACS Appl. Mater. Interfaces* **2019,** 11, (11), 10874-10882.

51. Zhao, M.; Wang, Y.; Ma, Q.; Huang, Y.; Zhang, X.; Ping, J.; Zhang, Z.; Lu, Q.; Yu, Y.; Xu, H.; Zhao, Y.; Zhang, H., Ultrathin 2D Metal–Organic Framework Nanosheets. *Adv. Mater.* **2015,** 27, (45), 7372-7378.

52. James, J. B.; Lin, Y., Kinetics of ZIF-8 thermal decomposition in inert, oxidizing, and reducing environments. *J. Phys. Chem. C* **2016,** 120, (26), 14015-14026.

53. Yin, H.; Kim, H.; Choi, J.; Yip, A. C. K., Thermal stability of ZIF-8 under oxidative and inert environments: A practical perspective on using ZIF-8 as a catalyst support. *Chem. Eng. J.* **2015,** 278, 293-300.

54. Zhu, W.; Li, X.; Sun, Y.; Guo, R.; Ding, S., Introducing hydrophilic ultra-thin ZIF-L into mixed matrix membranes for $CO_2/CH_4$ separation. *RSC Advances* **2019,** 9, (40), 23390-23399.

55. Ahn, J.; Chung, W.-J.; Pinnau, I.; Guiver, M. D., Polysulfone/silica nanoparticle mixed-matrix membranes for gas separation. *J. Membr. Sci.* **2008,** 314, (1), 123-133.

56. Moaddeb, M.; Koros, W. J., Gas transport properties of thin polymeric membranes in the presence of silicon dioxide particles. *J. Membr. Sci.* **1997,** 125, (1), 143-163.

57. Rodenas, T.; van Dalen, M.; García-Pérez, E.; Serra-Crespo, P.; Zornoza, B.; Kapteijn, F.; Gascon, J., Visualizing MOF Mixed Matrix Membranes at the Nanoscale: Towards Structure-Performance Relationships in $CO_2/CH_4$ Separation Over $NH_2$-MIL-53(Al)@PI. *Adv. Funct. Mater.* **2014,** 24, (2), 249-256.

58. Potreck, J.; Nijmeijer, K.; Kosinski, T.; Wessling, M., Mixed water vapor/gas transport through the rubbery polymer PEBAX® 1074. *J. Membr. Sci.* **2009,** 338, (1), 11-16.

59. Rezac, M. E.; John, T.; Pfromm, P. H., Effect of copolymer composition on the solubility and diffusivity of water and methanol in a series of polyether amides. *J. Appl. Polym. Sci.* **1997,** 65, (10), 1983-1993.

60. Liu, G.; Jiang, Z.; Cao, K.; Nair, S.; Cheng, X.; Zhao, J.; Gomaa, H.; Wu, H.; Pan, F., Pervaporation performance comparison of

hybrid membranes filled with two-dimensional ZIF-L nanosheets and zero-dimensional ZIF-8 nanoparticles. *J. Membr. Sci.* **2017,** 523, 185-196.

61. Yu, B.; Cong, H.; Li, Z.; Tang, J.; Zhao, X. S., Pebax-1657 nanocomposite membranes incorporated with nanoparticles/colloids/carbon nanotubes for $CO_2/N_2$ and $CO_2/H_2$ separation. *J. Appl. Polym. Sci.* **2013,** 130, (4), 2867-2876.

62. Surya Murali, R.; Ismail, A. F.; Rahman, M. A.; Sridhar, S., Mixed matrix membranes of Pebax-1657 loaded with 4A zeolite for gaseous separations. *Sep. Purif. Technol.* **2014,** 129, 1-8.

63. Zhao, D.; Ren, J.; Li, H.; Li, X.; Deng, M., Gas separation properties of poly(amide-6-b-ethylene oxide)/amino modified multi-walled carbon nanotubes mixed matrix membranes. *J. Membr. Sci.* **2014,** 467, 41-47.

64. Jomekian, A.; Behbahani, R. M.; Mohammadi, T.; Kargari, A., Utilization of Pebax 1657 as structure directing agent in fabrication of ultra-porous ZIF-8. *J. Solid State Chem.* **2016,** 235, 212-216.

65. Dong, G.; Hou, J.; Wang, J.; Zhang, Y.; Chen, V.; Liu, J., Enhanced $CO_2/N_2$ separation by porous reduced graphene oxide/Pebax mixed matrix membranes. *J. Membr. Sci.* **2016,** 520, 860-868.

66. Dai, Y.; Ruan, X.; Yan, Z.; Yang, K.; Yu, M.; Li, H.; Zhao, W.; He, G., Imidazole functionalized graphene oxide/PEBAX mixed matrix membranes for efficient $CO_2$ capture. *Sep. Purif. Technol.* **2016,** 166, 171-180.

67. Xiang, L.; Pan, Y.; Zeng, G.; Jiang, J.; Chen, J.; Wang, C., Preparation of poly(ether-block-amide)/attapulgite mixed matrix membranes for $CO_2/N_2$ separation. *J. Membr. Sci.* **2016,** 500, 66-75.

68. Meshkat, S.; Kaliaguine, S.; Rodrigue, D., Mixed matrix membranes based on amine and non-amine MIL-53(Al) in Pebax® MH-1657 for $CO_2$ separation. *Sep. Purif. Technol.* **2018,** 200, 177-190.

69. Sutrisna, P. D.; Hou, J.; Zulkifli, M. Y.; Li, H.; Zhang, Y.; Liang, W.; D'Alessandro, Deanna M.; Chen, V., Surface functionalized UiO-66/Pebax-based ultrathin composite hollow fiber gas separation membranes. *J. Mater. Chem. A* **2018,** 6, (3), 918-931.

70. Aghaei, Z.; Naji, L.; Hadadi Asl, V.; Khanbabaei, G.; Dezhagah, F., The influence of fumed silica content and particle size in poly (amide 6-b-ethylene oxide) mixed matrix membranes for gas separation. *Sep. Purif. Technol.* **2018,** 199, 47-56.

71. Xiang, L.; Pan, Y.; Jiang, J.; Chen, Y.; Chen, J.; Zhang, L.; Wang, C., Thin poly(ether-block-amide)/attapulgite composite membranes with improved $CO_2$ permeance and selectivity for $CO_2/N_2$ and $CO_2/CH_4$. *Chem. Eng. Sci.* **2017,** 160, 236-244.

72. Shen, J.; Liu, G.; Huang, K.; Jin, W.; Lee, K.-R.; Xu, N., Membranes with Fast and Selective Gas-Transport Channels of Laminar Graphene Oxide for Efficient $CO_2$ Capture. *Angew. Chem.* **2015,** 127, (2), 588-592.

73. Shen, Y.; Wang, H.; Zhang, X.; Zhang, Y., $MoS_2$ Nanosheets Functionalized Composite Mixed Matrix Membrane for Enhanced $CO_2$ Capture via Surface Drop-Coating Method. *ACS Appl. Mater. Interfaces* **2016,** 8, (35), 23371-23378.

Table of Contents